Earth Surf. Dynam., 10, 191–208, 2022
https://doi.org/10.5194/esurf-10-191-2022

Earth Surface Dynamics
Open Access
EGU

Rapid Holocene bedrock canyon incision of Beida River, North Qilian Shan, China

Yiran Wang[1,2], Michael E. Oskin[1], Youli Li[3], and Huiping Zhang[4]

[1]Department of Earth and Planetary Sciences, University of California, Davis, California, USA
[2]Earth Observatory of Singapore, Nanyang Technological University, Singapore
[3]College of Urban and Environmental Sciences, Peking University, Beijing, China
[4]Institute of Geology, China Earthquake Administration, Beijing, China

Correspondence: Yiran Wang (yrwwang@ucdavis.edu)

Received: 6 June 2021 – Discussion started: 12 July 2021
Revised: 2 December 2021 – Accepted: 11 February 2022 – Published: 14 March 2022

Abstract. Located at the transition between monsoon- and westerly-dominated climate systems, major rivers draining the western North Qilian Shan incise deep, narrow canyons into latest Quaternary foreland basin sediments of the Hexi Corridor. Field surveys and previously published geochronology show that the Beida River incised 130 m at the mountain front over the Late Pleistocene and Holocene at an average rate of 6 m kyr^{-1}. We hypothesize that a steep knickzone, with 3 % slope, initiated at the mountain front and has since retreated to its present position, 10 km upstream. Additional terrace dating suggests that this knickzone formed around the mid-Holocene, over a duration of less than 1.5 kyr, during which incision accelerated from 6 m kyr^{-1} to at least 25 m kyr^{-1}. These incision rates are much faster than the uplift rate across the North Qilian fault, which suggests a climate-related increase in discharge drove rapid incision over the Holocene and formation of the knickzone. Using the relationship between incision rates and the amount of base level drop, we show the maximum duration of knickzone formation to be $\sim$ 700 years and the minimum incision rate to be 50 m kyr^{-1}. We interpret that this period of increased river incision corresponds to a pluvial lake-filling event at the terminus of the Beida River and correlates with a wet period driven by strengthening of the Southeast Asian Monsoon.

1 Introduction

An incising river responds to tectonic or climatic perturbation by adjusting its slope, expressed by formation of knickpoints or knickzones (Crosby and Whipple, 2006; Tucker and Whipple, 2002; Whittaker, 2012), and through changes of its channel width (Finnegan et al., 2005). Understanding the evolution and migration of knickzones, channel width, and the coupling between these adjustments is important in unraveling the type, duration, and amplitude of a perturbation (Attal et al., 2011; Berlin and Anderson, 2007; Bishop et al., 2005). Previous studies on headward-migrating knickpoints focus on the role of tectonic uplift or a base level fall and usually regard climate conditions and channel width as constant (e.g., Tucker and Whipple, 2002; Crosby and Whipple, 2006; Haviv et al., 2006; Wobus et al., 2006). Here we present a case of steep, quickly retreating knickzones within the western North Qilian Shan, formed under the combined influence of climatic change and lithologic control. Through modeling of incision of the Beida River, as recorded by its profile and stream terraces preserved along its course, we suggest this knickzone was formed during a short period, 4000–5000 years before present, under an exceedingly fast incision rate. This is most likely to be the result of an increase in river discharge, and perhaps a commensurate decrease in sediment supply.

In western China, the North Qilian Shan is the source of several northeastward-flowing rivers with deep canyons incised across the mountain–basin boundary (Fig. 1a). In the western North Qilian Shan, three major tributaries of the Hei He drainage, Maying, Hongshuiba, and Beida, carve deep canyons into the foreland sediments and across the fault-controlled boundary with the bedrock hinterland, forming

prominent knickzones within the hinterland that are tens of meters high (Fig. 1b–d). As one of these deeply incised rivers, the Beida River is characterized by a prominent knickzone which separates its profile into three patches (upper patch 1, knickzone patch 2, and lower patch 3; Fig. 2a). Each patch can be distinguished by different channel slopes and channel widths: gentle and wide upper patch, steep and narrow knickzone, and a lower patch with a gentle slope similar to the upper patch, but a narrower channel. The successive generation and retreat of these patches correspond to different boundary conditions (see Royden and Perron, 2013) and together record the incision history at the mountain front.

2 Geological background

The Qilian Shan form the northeastern margin and the youngest growing portion of the Tibetan Plateau (Tapponnier et al., 2001). Thermochronology studies suggest that uplift of the North Qilian Shan commenced around the mid-Miocene, with an exhumation rate of $\sim 1\,\mathrm{m\,kyr^{-1}}$ (Jolivet et al., 2001; Zheng et al., 2010; He et al., 2017, 2021). The Hexi Corridor, north of the Qilian Shan, consists of a chain of foreland basins. Bordering arid central Asia, the Qilian Shan and Hexi Corridor occupy the transition zone between Southeast Asian Monsoon and westerlies (An et al., 2001; Wei and Gasse, 1999). The monsoon brings summer rain inland while the mid-latitude westerlies bring dry air and a small amount of water vapor in winter. Monsoon influence diminishes and annual precipitation declines from east to west, both within the Hexi Corridor and at high altitudes within the Qilian Shan (Meng et al., 2012; Shi et al., 2006). At the mountain front bounding the western Hexi Corridor, the annual precipitation declines from 200–300 mm $\mathrm{yr^{-1}}$ at the Maying River to 100–200 mm $\mathrm{yr^{-1}}$ at the Beida River. At high altitudes (>4000 m) within the western North Qilian Shan, there is a similar annual precipitation gradient from east to west, from 300–400 to 200–300 mm $\mathrm{yr^{-1}}$ (Qiang et al., 2016; Geng et al., 2017). The maxima of precipitation occur at approximately 4200 m elevation (Chen et al., 2018). The modern glacial-equilibrium altitude line of the Qilian Shan increases from 4400 to 5000 m from northeast to southwest (Shi, 2011), reflecting the westward decrease in precipitation. Between the years 2005 and 2010, within the Qilian Shan there were 2684 glaciers with a total area of 1600 $\mathrm{km^2}$ and an ice volume of 84 $\mathrm{km^3}$ (Guo et al., 2014; Sun et al., 2015). These glaciers covered approximately 4 % of the landscape above 4000 m elevation. The extent of these glaciers has fluctuated repeatedly throughout the Quaternary. Dating of moraines suggests that glacial advances have occurred during the little ice age ($\sim$ 1300–1850 AD), MIS (Marine Isotope Stage) 2, MIS 4, MIS 6, and MIS 12; some glacial expansion may have occurred during MIS 3 as well (Shi et al., 2006). The glacial equilibrium line altitude of Qilian Shan during the Last Glacial Maximum (LGM) is estimated to be as much as 400 m lower than present (Hu et al., 2014; Owen et al., 2003; Shi et al., 2006; Zhao et al., 2001; Zhou et al., 2002).

The Hei He forms the largest drainage basin in the North Qilian Shan and terminates within the Juyanze paleolake basin, north of the Hexi Corridor. Sediment and core records from the Juyanze paleolake basin indicate frequent dry–wet oscillations over the past 11 000 years (Hartmann and Wünnemann, 2009; Herzschuh et al., 2004; Mischke et al., 2002, 2005). The highest lake level occurred during the early Holocene (10700–8900 yr BP, $\sim$ 20 m deep), and the highest mid-Holocene lake level ($\sim$ 15–17 m deep) occurred during 5400–3900 yr BP and peaked at about 4200 yr BP (East Juyanze lake, Hartmann and Wünnemann, 2009).

Three major tributaries, Beida, Hongshuiba, and Maying, join the Hei He from the south and west (Fig. 1, Table 1). In the hinterland, the three rivers flow through Pre-Cambrian and Paleozoic meta-sedimentary and meta-igneous rocks (Fig. S1 in the Supplement); in the foreland, these rivers deposit sediments into the Hexi Corridor basins. The North Qilian range overthrusts the southern margin of the Hexi Corridor, placing metasedimentary rocks against the Quaternary basin deposits. Presently, the channels of the Maying, Hongshiba, and Beida rivers have incised deeply into Late Pleistocene alluvial fans of the proximal foreland basin and into correlative fill terraces and bedrock within the range (Hetzel et al., 2019; Yang et al., 2020; Wang et al., 2020), forming a prominent knickzone along each river located $\sim$ 7–13 km upstream of the mountain front (Fig. 1b–d). The canyons of the three rivers are deepest at the mountain front where the North Qilian fault juxtaposes bedrock against Quaternary sediments, $\sim$ 130, $\sim$ 190, and $\sim$ 240 m for Beida, Hongshuiba, and Maying rivers, respectively (Fig. S2). The depths of these river canyons gradually decrease basinward until 25–30 km downstream, where the rivers form active alluvial fans.

Along the Beida River, at least two generations of fill terraces (T1 and T2) are preserved well and continuously in the hinterland and extend to the foreland basin. Our previous research (Wang et al., 2020) suggests that T1 was abandoned after 24 ± 3 kyr BP, during the last glacial period; T2 was abandoned after 144 ± 30 kyr BP, during the penultimate glacial period. Flights of terraces inset below both T1 and T2 terrace treads mark progressive degradation of the terrace fill and incision into underlying bedrock. Along the mountain front, strands of the North Qilian fault cut the terraces of Beida River, offsetting T1 and T2 vertically by 15 and > 60 m, respectively. In the hinterland, the T2 terrace profile reveals a long wavelength fold ($\sim$ 30 km) with maximum uplift of $\sim$ 120 m relative to T1. Combined, the fault offset and folding indicate a maximum uplift rate of $\sim 1\,\mathrm{m\,kyr^{-1}}$ at the fold crest, and a horizontal shortening rate of $1.4 \pm 0.4\,\mathrm{m\,kyr^{-1}}$ across the North Qilian Shan (Wang et al., 2020).

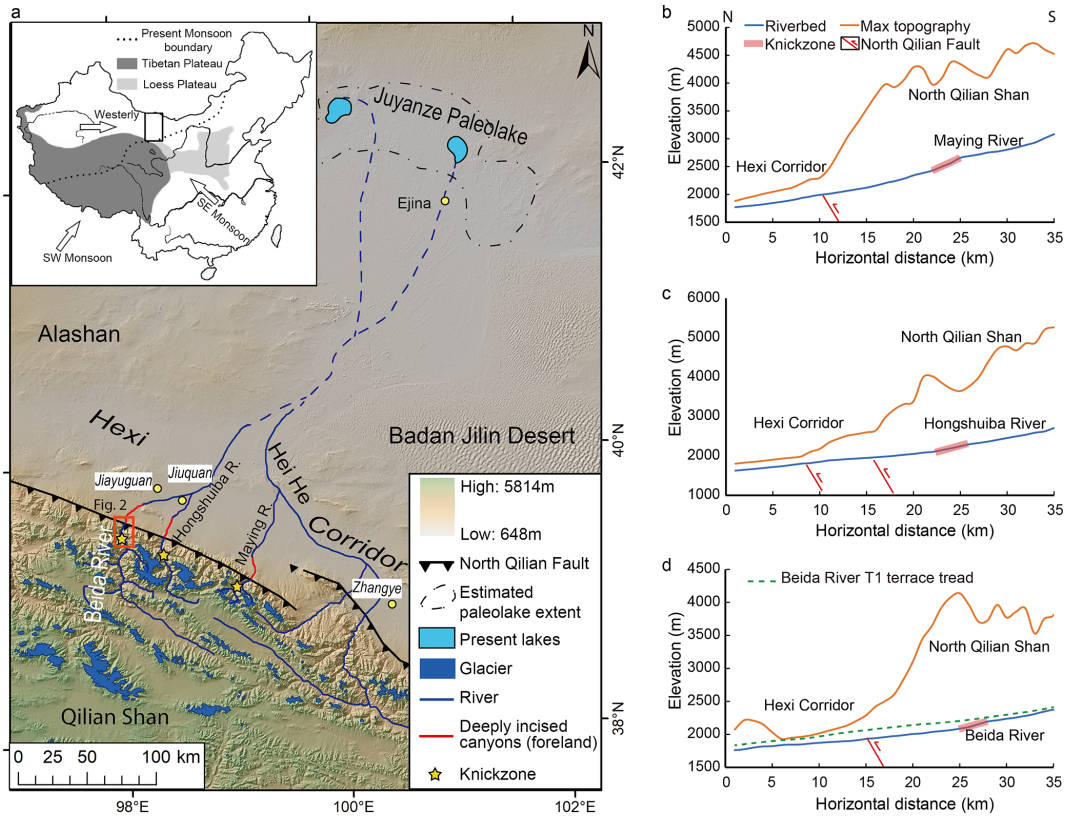

Figure 1. **(a)** Digital elevation map of the Hei He drainage system. Active glacial coverage map based on Raup et al. (2007). Inset figure: location with respect to monsoon and westerly moisture sources. **(b–d)** River and maximum elevation profiles of three major tributaries of the Hei He drainage, extracted from 30 m SRTM. Maximum elevation sampled from swaths 16 km in width, centered on each river. Locations of active strands of the North Qilian fault denote foreland-hinterland junction at mountain front. All three rivers exhibit deep incision below the top of foreland-basin sediments. Red highlights knickzone reach within bedrock. Dashed line in **(d)** is reconstructed profile of the Beida River from the ca. ∼ 24 ka T1 terrace tread, prior to onset of rapid incision phase.

Table 1. Hydrological information of the three major rivers draining the western North Qilian Shan (Gansu Province Local Chronicles Compilation Committee, 1998).

	Length (km)	Drainage area (km^2)	Annual discharge ($\times 10^8$ m^3)	Glacial coverage (km^2); contribution to annual discharge
Beida	243	6910	6.53	137; 16 %
Hongshuiba	87	1580	2.87	131; 35 %
Maying	34	619	1.16	20; 12 %

3 Methods

3.1 Field survey

The late Pleistocene T1 fill terrace, up to 60–80 m thick, is preserved continuously along the narrow bedrock gorge of the Beida River. This terrace grades to an extensive alluvial fan deposit emanating from the mountain front, with minor disruption from reverse fault offsets (Fig. 2). The Beida river gorge cuts across the fault-controlled basin boundary, forming a narrow slot canyon up to 125 m deep within the foreland-basin fan gravels. We mapped and surveyed the terrace sequence and the course of Beida River inside the mountain range using a laser rangefinder (∼ 0.3 m distance accuracy, 0.25° inclination accuracy) and differential GPS. Wherever possible, the terrace tread (top of the fluvial gravel), terrace strath (base of fluvial gravel), and present riverbed were measured together (Fig. 3, Table S1). In the foreland, we extract terrace elevations and the river profile from an 8 m resolution digital elevation model produced by the Polar Geospatial Center (Shean, 2017). For the hinterland tributaries, we extract river profiles from the same 8 m resolution digital elevation model (DEM). Present bedrock channel

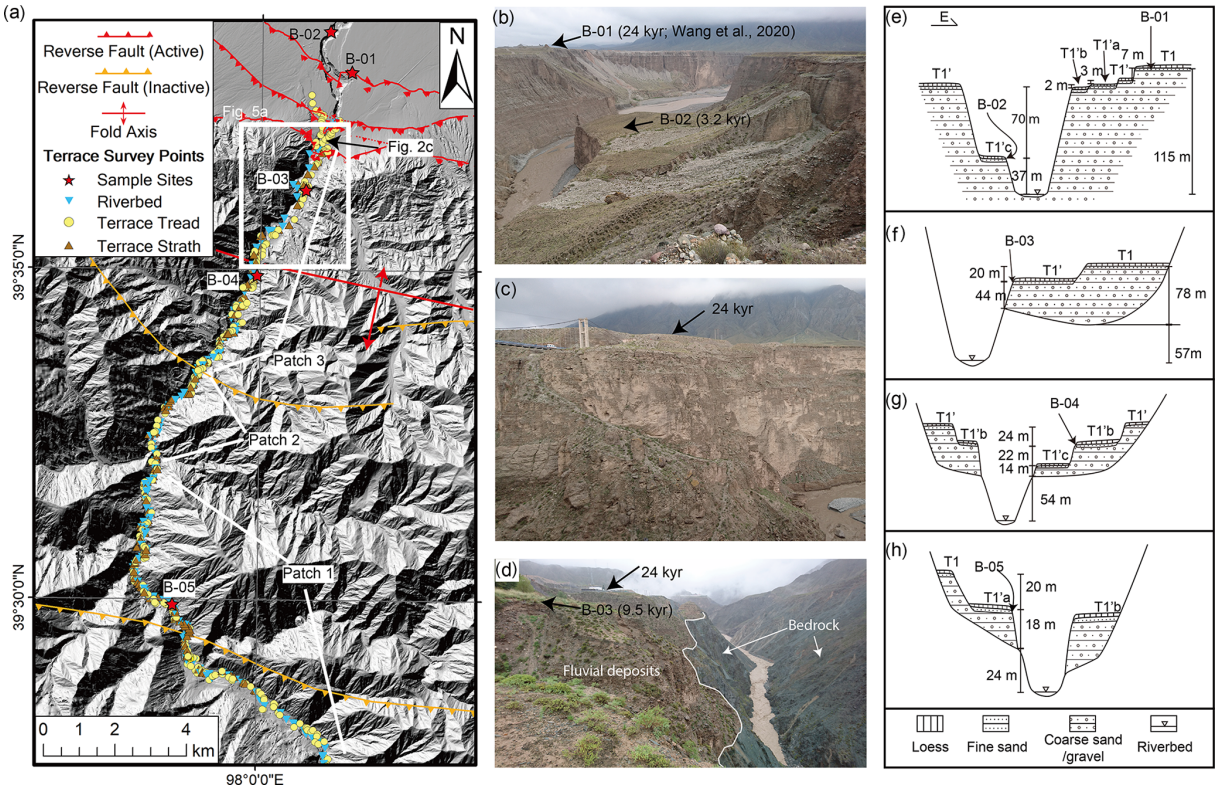

Figure 2. **(a)** Map of the Beida River within the North Qilian Shan, with survey points and geochronology sample sites indicated. **(b)** Photo of Beida River canyon and sample site B-01 AND B-02 within the foreland, looking upstream. Thick layers of gravel are exposed on the canyon walls. **(c)** Photo of Beida River canyon and T1 terraces near the mountain front, looking east (location in Fig. 2a). In this photo, the 24 kyr T1 terrace tread is ∼ 40 m above the 9.5 kyr T1' terrace tread. **(d)** Photo of Beida River canyon and sample site B-03 inside the mountains, looking upstream. This photo shows that the Beida River deeply incises into the bedrock below the terrace fill. **(e–h)** Cross sections of the Beida River terraces at each sample site, facing downstream. Note that labels a, b, and c indicate local terrace ordering and cannot be directly correlated to terraces upstream and downstream.

widths were measured from Google Earth imagery at 100 m intervals along the river course. We measured the width of the water surface from imagery acquired during the wet season, mostly between July and September 2010 to 2016. Due to limited data availability, a few measurements were obtained from imagery acquired in May and October (Table S2).

3.2 Geochronology

The abandonment age of T1 was dated to be 24 ± 3 kyr by combining optically stimulated luminescence (OSL) and terrestrial cosmogenic nuclide (^{10}Be) exposure ages (Fig. 2, sample site B-01; Wang et al., 2020). To document the post-24 kyr incision history of Beida River within the hinterland, we collected charcoal samples from the fine sand and silty overbank deposits on three inset terraces (Fig. 2; sample sites B-03, B-04, B05; Fig. S3). These overbank deposits were deposited after terrace formation, but before incision was sufficient to isolate the terrace surface from flood events. At one site within the foreland basin, we collected an OSL sample from the bottom of the loess covering a low inset terrace (Fig. 2, sample site B-02). A total of 10 charcoal samples were measured at the Keck Carbon Cycle AMS Facility at UC Irvine. The results were calibrated with an IntCal13 calibration curve (Reimer et al., 2013) (Table 2). The OSL sample (BD-O-12) was processed and measured at the State Key Laboratory of Earthquake Dynamics, China Earthquake Administration. The equivalent doses (De) for the pure fine-grained quartz were determined by the simplified multiple aliquot regenerative-dose (SMAR) protocol (Tables 3 and S3, Fig. S4).

3.3 Bedrock incision model

We apply the concept of slope patches (Royden and Perron, 2013) to model the evolution of the Beida River stream profile. The formation of a slope patch is based on stream power, which has the form

$$\frac{\mathrm{d}z}{\mathrm{d}t} = K\left(\frac{QS}{W}\right)^{n}, \tag{1}$$

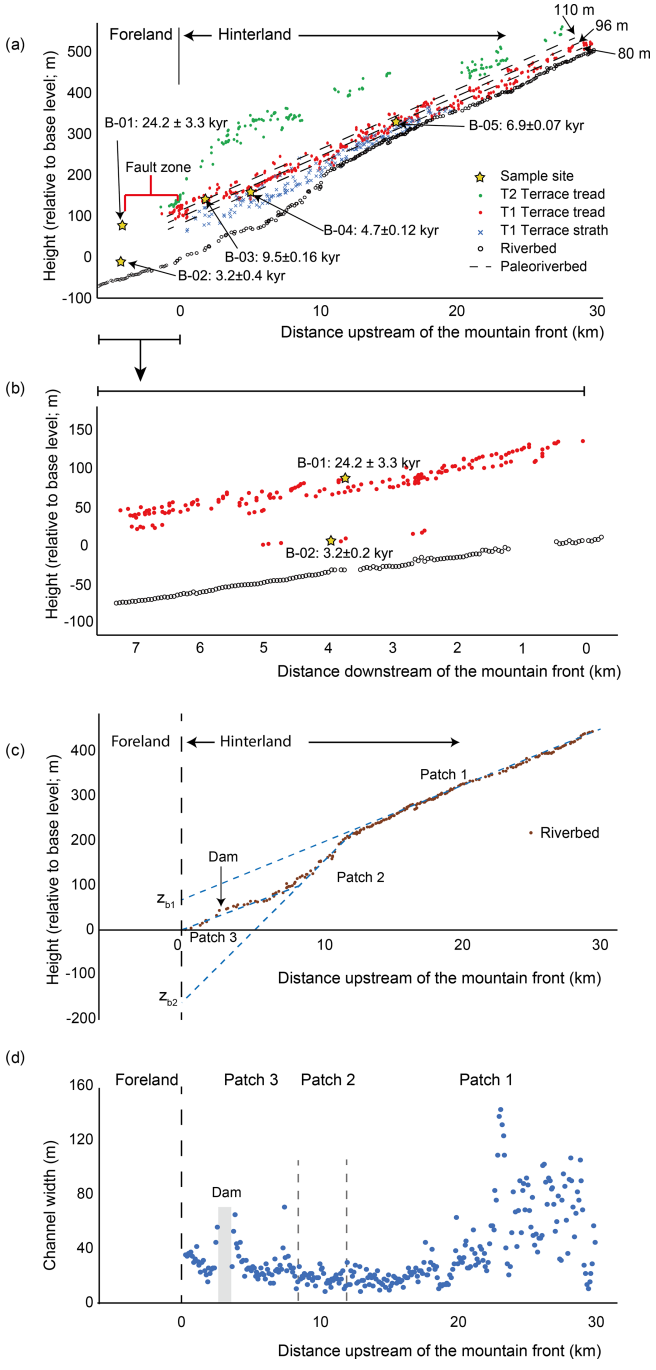

Figure 3. **(a)** Longitudinal profile of the Beida River channel, with terrace treads (T2, T1, and all T1 inset terrace treads) and strath elevations; sample sites and ages (expressed at the 2σ confidence level) also indicated. Dashed lines are inferred prior river profiles corresponding to the sample site elevations, with the relative height above present base level annotated (not corrected for tectonic uplift). **(b)** Terrace elevations (red) and channel elevations (open circles) along the Beida River within the foreland basin. Note sparse terrace record below T1 and T1'. **(c)** Three patches of Beida river profile, projected to effective base level at the mountain front. **(d)** Present bedrock channel width measured at 100 m intervals along the course of the Beida River. The width measurements that are within $\sim$ 500 m upstream and downstream of the dam are excluded.

Table 2. ^{14}C age of Beida River terraces.

Sample site*	Coordinates	Sample name	Modern fraction	±	$D^{14}C$ (‰)	±	^{14}C age (BP)	±	Calibrated age 1σ (BP)	Calibrated age 2σ (BP)
B-03 (T1'; 115 m)	39.60126°, 98.01365°	BDC-3	0.3462	0.0028	−653.8	2.8	8520	70	9473–9544	9332–9340 9404–9632 9645–9657
		BDC-4	0.3393	0.0008	−660.7	0.8	8680	20	9557–9630 9647–9653	9552–9679
		BDC-5	0.3378	0.0008	−662.2	0.8	8720	20	9611–9699	9561–9737
		BDC-6	0.3320	0.0009	−668.0	0.9	8855	25	9895–9949 9990–10012 10 025–10 038 10 061–10 134	9784–9848 9861–9878 9883–9966 9982–10 155
B-04 (T1'b; 90 m)	39.57600°, 97.99493°	BDC-8	0.5973	0.0011	−402.7	1.1	4140	15	4617–4652 4669–4703 4757–4765 4784–4809	4580–4726 4752–4770 4780–4815
		BDC-9	0.5715	0.0011	−428.5	1.1	4495	20	5054–5077 5105–5136 5163–5189 5213–5228 5231–5251 5257–5281	5047–5147 5153–5202 5210–5288
		BDC-10	0.5862	0.0011	−413.8	1.1	4290	15	4844–4856	4839–4862
B-05 (T1'a; 42 m)	39.498771°, 97.971940°	BDC-11	0.4702	0.0012	−529.8	1.2	6060	20	6893–6944	6807–6811 6856–6979
		BDC-12	0.4497	0.0029	−550.3	2.9	6420	60	7309–7419	7185–7186 7246–7439
		BDC-14	0.4725	0.0010	−527.5	1.0	6025	20	6800–6815 6845–6901	6797–6934

*Inside the bracket shows the terrace that the sample collected from, and the height of the terrace above the riverbed. Note that labels a and b indicate local terrace ordering and cannot be correlated to terraces upstream and downstream.

Table 3. OSL age of loess covering terrace tread.

Sample site	Sample name[1]	Coordinates	U ppm^{-1}	Th ppm^{-1}	K (%)	Water content (%)	Dose rate (Gy ka^{-1})	Equivalent dose[1] (Gy)	Age[2] (ka)
B-02	BD-O-12	98.02299, 39.64376	2.34 ± 0.10	9.32 ± 0.28	1.67 ± 0.06	0	3.5 ± 0.3	11.4 ± 0.7	3.2 ± 0.2

[1] Grain size < 100 µm.
[2] Uncertainties in equivalent dose, dose rate, and age determinations are expressed at the 1σ confidence level.

where z is the channel elevation, t is time, Q is river discharge, S is channel slope, W is channel width, and K and n are an empirical erosional efficiency and exponent, respectively (Tucker and Whipple, 2002; Whipple and Tucker, 1999).

A slope patch forms in the bedrock channel immediately upstream of the channel outlet, with channel slope that develops in balance with the rate of base-level fall. Setting $\frac{dz}{dt}$ to the incision rate, I, at the mountain front, we rearrange Eq. (1) to solve for this channel slope:

$$S = \left|\frac{dz}{dx}\right| = \left(\frac{I}{K}\right)^{\frac{1}{n}} \left(\frac{W}{Q}\right). \quad (2)$$

For the case of the Beida River, no major tributary enters along its lower 30 km long course; the drainage area of the Beida River, measured from 30 m SRTM (Shuttle Radar Topography Mission) DEM, at the river outlet (mountain front) is $\sim 6.91 \times 10^9$ km^2, while the drainage area above the knickzone is $\sim 6.84 \times 10^9$ km^2, a difference of ~ 1 %. Thus, we assume that Q does not vary spatially along the channel course and may be treated as constant over an incision phase, though it may vary from one phase to the next. We also assume that channel width (W) remains constant within a given slope patch. During formation of a slope patch, river profile elevation is thus found by integrating Eq. (2) over its finite span x_b to x:

$$z(x) = \left(\frac{I}{K}\right)^{\frac{1}{n}} \left(\frac{W}{Q}\right)(x - x_b) + z_b = S(x - x_b) + z_b, \quad (3)$$

where x_b and z_b are the horizontal position and elevation at base level, respectively. We define base level as the bedrock-basin transition at the mountain front.

We model the bedrock incision history of the Beida river as a consequence of varying incision rate over time at base level. Once formed, a slope patch behaves as a kinematic wave, retaining its gradient as it retreats upstream (Perron and Royden, 2013). The elevation of the $(n-1)$th slope patch (the patch formed one stage before present) may thus be cast as a function of its slope during formation, $S_{(n-1)}$, and an effective base-level elevation $z_{b(n-1)}$ of the slope patch projected to the outlet position. This base level may be predicted by correcting the present base level elevation, z_b, by the difference in the amount of incision across neighboring patches n and $n-1$,

$$z_{b(n-1)} = z_b + \left(I_{n,j} - I_{n-1,j}\right) t_j. \quad (4)$$

$I_{n,j}$ is the incision rate of patch n, currently being formed during time interval t_j, directly upstream of the outlet. $I_{n-1,j}$ is the incision rate of patch $n-1$ during that time interval t_j. Note that this incision rate may be different from the incision rate during formation of patch $n-1$ (i.e., faster for an increase in discharge). However, varying discharge over time is not required for our model, only changes of channel slope driven by varying the incision rate at the mountain front. For the $(n-2)$th patch, the effective base level contains two correction terms (see z_{b1}, z_{b2} of Fig. 3c),

$$z_{b(n-2)} = z_b + \left(I_{n,j} - I_{n-2,j}\right) t_j + \left(I_{n-1,j-1} - I_{n-2,j-1}\right) t_{j-1}. \quad (5)$$

This may be generalized to additional slope patches, each corrected by the incision rate differences between patches. We apply Eqs. (4) and (5), combined with the incision recorded in stream terraces adjacent to the Beida River, to constrain its incision-rate history. Note that Eqs. (4) and (5) are derived on the premise that discharge (Q) is constant during each incision phase, and that channel width (W) may vary between different patches but remains constant within a patch – i.e., that Eq. (3) is valid.

4 Results

4.1 Beida River profiles

Presently, the 30 km reach of the Beida River upstream of the mountain front is entirely contained within a bedrock channel. Channel slopes, measured directly from fitting the long profile, show a knickzone between 10 and 12 km upstream of the mountain front (Fig. 3). The knickzone divides the river profile into three patches: patch 1, upstream of the knickzone, with a slope of 0.013; patch 2, the knickzone itself, with a slope of 0.029; patch 3, below the knickzone with a slope of 0.012 (Fig. 3c). Channel width also varies along the course of the Beida River. In patch 1, the channel width ranges between 14 and 140 m, with an average of 43 m; in patch 2, the channel width ranges between 8 and 29 m, with an average of 17 m; in patch 3, the channel width ranges between 14 and 70 m, with an average of 30 m (Fig. 3d). In the foreland, the river incises into the 24 kyr T1 terrace, which is part of an extensive alluvial fan surface. The river canyon is deepest at the mountain front, and its depth gradually decreases downstream, indicating a decrease in river gradient within the foreland from 24 kyr BP to present. Near the mountain front, the slope of the riverbed is presently ~ 0.010, while the slope of the adjacent alluvial fan surface is ~ 0.013.

Major tributaries of the Beida River all have knickpoints at their junction with the main stem (Fig. 4). Below the main-stem knickzone, these tributary knickpoints are mostly over 100 m high and form waterfalls. Above the main stem knickzone, the tributary knickzones are steep but graded to the main stem, and only half as high as those downstream of the main-stem knickzone. By projecting the tributary profiles to the main stem, we find that the tributary junctions define a single, graded main-stem profile without evidence for a knickzone (Fig. 4).

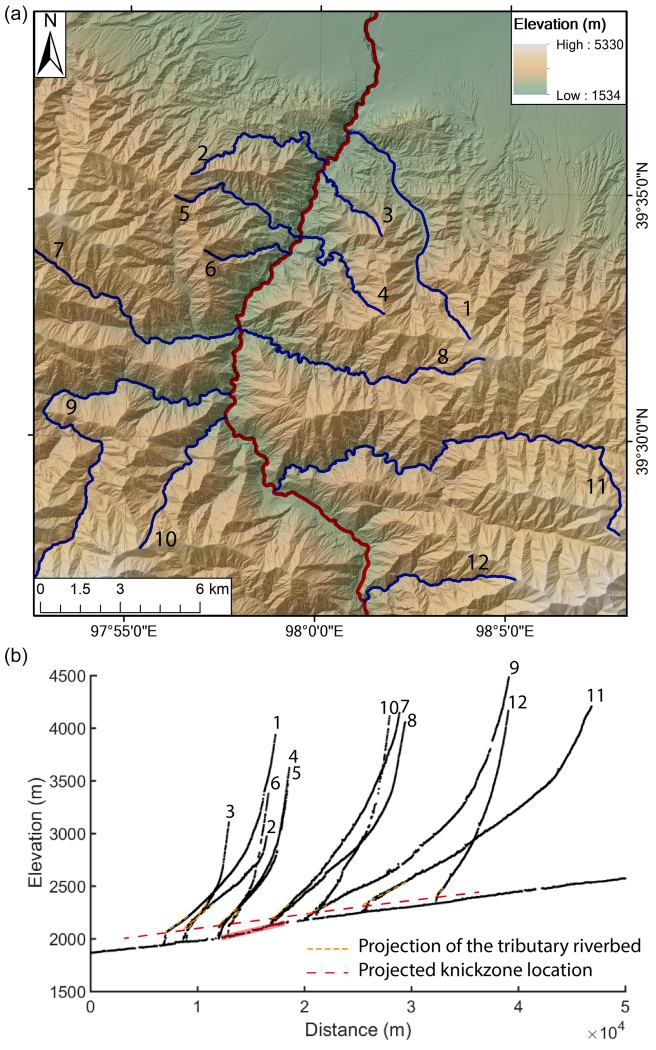

Figure 4. **(a)** Map of the tributaries of the Beida River. Red delineates the main stem; blue delineates tributaries. **(b)** Longitudinal profiles of the tributaries of the Beida River, as numbered in **(a)**. The main-stem knickzone is highlighted in red. Dashed red line connects the projection of tributary streams to the junction with the main stem based on stream gradient above each tributary knickzone.

4.2 Beida River terrace development

North of the mountain front, the 24 kyr T1 fill terrace merges into the extensive T1 alluvial fan. Though the river has incised an over 100 m deep canyon, no bedrock is exposed in the foreland. Within the mountain range, the T1 fill ranges from 60 to 80 m of thickness and consists of unconsolidated medium to poorly sorted, well-rounded boulder-cobble conglomerate and sandy conglomerate. The lithology of the sediments mainly consists of quartzite, granite, slate, and limestone. T1 treads are very well preserved, only covered by a 1–2 m loess cap except at tributary junctions, where alluvial fans are deposited upon the tread. The T1 tread presently lies ∼ 115 m above the riverbed immediately north of the northernmost strand of the North Qilian fault, ∼ 125–130 m above the present riverbed of patch 3 at the mountain front, up to ∼ 130–135 m above the patch 3 upstream of the mountain front, and ∼ 60 m above the riverbed of patch 1. Bedrock below the T1 strath is exposed continuously in the hinterland for at least 30 km along the Beida River. The most prominent inset (cut) terrace, T1', is preserved continuously at an elevation 7 to 20 m lower than T1 tread, both inside the mountain range and in the foreland basin. ^{14}C dating of charcoal samples at site B-03 (Figs. 2a, f and 3a) indicates abandonment of T1' occurred after 9.5 ± 0.16 kyr BP. Several levels of local inset (cut) terraces are preserved along the river, generally between a few meters and ∼ 40 m below the T1' tread. Different from T1 and T1' terraces, these inset terraces are local features formed as the river incised and meandered (Merritts et al., 1994), and therefore it is difficult or impossible to correlate these to other terraces upstream and downstream. All inset terraces are cut into the T1 fill. No inset terraces appear to have been formed as the river cut below the level of the T1 fill. On top of all the inset terrace treads is 0.5 to 1 m thick fine sand layers with small gravel (< 10 mm) layers in between, which we interpret as overbank sediments deposited during floods soon after the terrace surface was abandoned. Loess, 0.5 to 1.5 m thick, is deposited atop the overbank deposits.

Selected inset terraces were dated to constrain the incision history of the Beida River. An inset terrace at site B-05, situated 42 m above the present riverbed of patch 1, yields an age of 6.9 ± 0.07 kyr (Figs. 2a, h, and 3a, Table 2). At site B-04, an inset terrace with tread elevated 90 m above the patch 3 riverbed and ∼ 24 m below the T1' tread yields an age of 4.7 ± 0.12 kyr (Figs. 2a, g, and 3a, Table 2). In the foreland, a suite of terraces was formed as the river first incised into the basin deposits. Here T1' and other younger inset terraces occur between 7 and 30 m below the T1 tread and 80 to 100 m above the present river level. Terraces are absent between 80 m and ∼ 30–40 m above the riverbed (Fig. 3a, b). An OSL sample collected from basal loess capping an inset terrace tread, 37 m above the present riverbed, yielded an age of 3.2 ± 0.40 kyr (site B-02 of Figs, 2a, e and 3a; Table 3).

We find that the Beida River incised its present bedrock gorge adjacent to its former canyon filled by T1. This appears to have started with formation of the T1' terrace at 9.5 kyr. Upstream of the mountain front, the T1' terrace tread is preserved continuously on the east bank for 3.6 km, while only bedrock is exposed on the west bank. Though the T1 terrace fill is up to ∼ 60–80 m thick in this area, bedrock is exposed in the canyon walls 10 to 15 m below T1' and 20 to 30 m below the top of the T1 fill. Farther upstream, mapped exposures show that the entire paleochannel fill has been preserved beneath T1 and T1' for several channel reaches (Figs. 5, S5).

4.3 Incision rate estimation with terrace records

The incision rate at the mountain front may be calculated from the ages and relative heights of the T1 inset terraces. Because the sample sites are scattered along the river, the heights of these terraces cannot be compared directly. Instead, we reconstruct the elevation of the river channel at 9.5, 6.9, and 4.7 kyr BP, by projecting the channel profile through the three sample sites to the mountain front based on the slope of patch 1 (Fig. 3a). The heights of these paleochannels above the present riverbed elevation at the mountain front are 110, 96, and 80 m, respectively (Table 4). After correction for faulting at the mountain front and folding of the range interior (Wang et al., 2020), the elevations at the mountain front are 102, 89, and 75 m above the present riverbed, respectively (Table 4). For the foreland terraces, we project the 3.2 kyr terrace to the mountain front based on present alluvial channel slope, retaining an elevation of 37 m above the river. Because this terrace is located on the footwall of the North Qilian Fault, we do not apply an adjustment for tectonic uplift. We also do not correct this site for subsidence, because unlike for the hinterland, where we have good constraints on uplift from deformed terraces, we do not have a marker of subsidence of the foreland. Wang et al. (2020) estimated that tectonic subsidence is only a small fraction ($<10\,\%$) of the hanging wall uplift and thus such a correction would be less than 0.5 m for this terrace. For the 24 kyr T1 tread, we use the T1 height at the mountain front, 131 m. After adjusting for tectonic uplift (15 m), its corrected elevation is 116 m. With these adjusted terrace heights, we calculate the incision rate at mountain front between 24.2 and 9.5 kyr BP was $\sim 1\,\mathrm{m\,kyr^{-1}}$. The incision rate accelerated over much of the Holocene, from $\sim 5\,\mathrm{m\,kyr^{-1}}$ between 9.5 and 6.9 kyr BP, to $\sim 6\,\mathrm{m\,kyr^{-1}}$ between 6.9 and 4.7 kyr BP, and to $\sim 25\,\mathrm{m\,kyr^{-1}}$ between 4.7 and 3.2 kyr BP. The incision rate remains high, at $\sim 12\,\mathrm{m\,kyr^{-1}}$, from 3.2 kyr BP to present (Fig. 6). It is worth noting the 3.2 kyr terrace date is a minimum age, which may lead to overestimation of the post-3.2 kyr incision rate and underestimation of incision rate between 4.7 and 3.2 kyr. However, we consider the 3.2 kyr date to be a good estimate of the terrace age because loess has been deposited continuously in this area since at least the middle–early Holocene (Küster et al., 2006). We also note that samples from the loess cover on top of the T1 terrace tread at site B-01 yield ages of 5.7 and 6.5 kyr (Wang et al., 2020), which further supports that loess deposition began at this time.

5 Discussion

5.1 Channel width and bedrock incision rate

Drainage area, and thus discharge, does not appreciably change across our research area; however, the bedrock channel width varies widely, from over 100 m (patch 1) to as low as ~ 10 m (patch 2). Based on bedrock channel erosional mechanisms, the channel width should scale with discharge and channel slope (Finnegan et al., 2005, 2007; Lamb et al., 2015; Turowski et al., 2007; Wobus et al., 2006; Wohl and David, 2008). Though the narrowing of patch 2 and a clear, almost factor-of-two increase in the average width from patch 2 to patch 3 are both consistent with coupling of channel width and slope, it is obvious that the upper reach of the patch 1 is considerably wider than expected (Fig. 3d). In addition, the cause for narrowing of channel width on patch 1 over the 5 km reach upstream of the knickzone is also not clear. Increased flow velocity and shear stress immediately above the knickzone (Haviv et al., 2006) could contribute to this narrowing, though it is unlikely that such a hydraulic effect would extend for kilometers upstream. Another possibility is that the wider reach of the Beida River is a result of lateral incision and removal of a more extensive T1 terrace fill. Though bedrock is exposed in the channel throughout patch 1, T1 terraces are more extensively preserved along its widest reach.

Variations in channel width may exert as much influence as discharge on incision rate (Lavé and Avuoac, 2000). For the Beida River, we observe that patch 1 and patch 3 share similar channel slopes (Fig. 3c) but show a 2-fold difference in their incision rates (Fig. 6). We attribute this difference to the difference in average channel width between different patches (Fig. 3d). We suggest that the narrower average width of patch 3 focuses stream power and enhances incision rate relative to patch 1 (Eq. 1). This explanation is at odds, however, with the 5 km long narrower reach of patch 1, which by this reasoning should be incising as fast as patch 3. We speculate that this reach could reflect recent removal of the T1 terrace and focusing of the channel as it incises into bedrock. We note that the channel slope here is slightly steeper than upstream, which could indicate acceleration of incision rate. At present the terrace record is insufficient to test this hypothesis.

5.2 Beida River knickzone formation and incision stages

We interpret the knickzone of the Beida River as a migrating kinematic wave, related to an accelerated incision rate earlier in time and downstream of its present position. We suggest the Beida River knickzone formed in response to an abrupt change in the rate of base-level lowering (Whipple and Tucker, 1999). It is likely that the knickzone of the Beida River first formed at the mountain front, where bedrock is juxtaposed against Quaternary foreland-basin sediments by the North Qilian fault. The knickzone is hypothesized to have formed here as a response to increased incision rate into the foreland-basin sediments, thus lowering base level relative to the bedrock. The most likely cause for this increase in incision rate is a change in discharge during this time period, with perhaps a contribution from decreased sediment flux. Both mechanisms would increase transport capacity and

Table 4. Terrace ages and relative heights.

Terrace age[1] (kyr)	Original terrace height (projected to mountain front, m)	Tectonic uplift rate[2] ($m\,kyr^{-1}$)	Terrace height (adjusted based on tectonic uplift)	
			Relative to present riverbed at mountain front (m)	Relative to patch 1 (m)
24.2 ± 3.3	131 ± 3[a]	0.62 ± 0.08	116 ± 3	64 ± 3
9.5 ± 0.16	110 ± 2.7	0.86 ± 0.24	102 ± 5	50 ± 5
6.9 ± 0.07	96 ± 3.2	0.92 ± 0.25	89 ± 4.9	37 ± 5
4.7 ± 0.12	80 ± 2.4	1.08 ± 0.29	75 ± 3.8	23 ± 3.8
3.2 ± 0.4	37 ± 3	0	37 ± 3	–

[1] Terrace ages are expressed at the 2σ confidence level.
[2] Tectonic uplift rates at the sample site are calculated based on the folding and faulting data in Wang et al. (2020).
[a] Here we report the terrace height at mountain front instead of the projected height from the sample site.

promote incision of the unconsolidated foreland-basin sediments (Tucker and Whipple, 2002). We suggest a change of discharge (and/or decrease in sediment flux) and the change in erodibility from foreland sediments to hinterland bedrock are the two key factors contributing to knickzone formation here. Without a change of erodibility, an increase in discharge would lead to uniform incision (if discharge is spatially invariant) of the bedrock channel, and relaxation (lowering of the river gradient) for the alluvial channel. We hypothesize instead that exposure of bedrock within the channel at the fault contact with the foreland led incision of the unconsolidated foreland-basin sediments to outpace bedrock incision upstream, resulting in formation of the knickzone.

We can rule out the alternative hypothesis of tectonic uplift as a driver of the formation of the prominent knickzone (patch 2), for two reasons. First, judging by the continuity of the T1 terrace tread (Fig. 3a) and our field work (Wang et al., 2020; Fig. S6), we can rule out the presence of an active fault under the knickzone. Second, the rate of incision of the Beida River greatly exceeds the tectonic uplift rate. Based on our previous research (Wang et al., 2020), the average vertical uplift rate at the mountain front since the abandonment of T1 is only $\sim 0.6\,m\,kyr^{-1}$. Additional uplift occurs via folding within the hinterland, reaching a maximum of ~ 15 m for the T1 terrace (vertical displacement by the frontal fault excluded) at 5 to 10 km upstream of the range front. This folding contributes an additional $\sim 0.6\,m\,kyr^{-1}$ to the uplift rate. In addition, the long-term exhumation rate based on thermochronology is $\sim 1\,m\,kyr^{-1}$ (Zheng et al., 2010). In comparison, the average incision rate since the abandonment of T1 terrace (24.2 kyr) is $\sim 5.4\,m\,kyr^{-1}$, and the average incision rate since the abandonment of T1' (9.5 kyr) is $\sim 12\,m\,kyr^{-1}$, both much larger than the tectonic uplift or exhumation rate.

A second alternative hypothesis is that the Beida River knickzone formed at its present location, related either to a change in erodibility of bedrock or a major tributary confluence. Based on a drainage-area analysis, no major tributary confluence occurs at the knickzone location. The geologic map (Fig. S1) shows no significant lithology change under the present knickzone location, which suggests local variations of lithology are unlikely to have caused knickzone formation at its present position. In addition, if the knickzone of the Beida River were a persistent feature of the channel, evidence for a buried knickzone should be preserved in the strath (paleoriverbed) elevations beneath the T1 terrace. We find that T1 strath elevations show no such sign of a knickzone (Fig. 3a). Therefore, neither the regional context nor local incision history suggest the presence of a fixed knickzone, and this alternative hypothesis can also be ruled out.

Based on the calculated incision rates, we can divide the Beida River incision history since the abandonment of T1 into two major phases. The first phase is between 24 and 9.5 kyr BP with an average incision rate $\sim 1\,m\,yr^{-1}$ after correcting for tectonic uplift, representing a state close to equilibrium relative to the long-term uplift and exhumation rate of the North Qilian Shan. The second phase is between 9.5 kyr BP and present, with an average incision rate an order of magnitude larger than the previous phase, representing an accelerated incision state. During the first phase, the relatively slow incision rate allowed the Beida River to meander widely, not only in the foreland but also within its hinterland canyon. This meandering resulted in widening of the canyon as the river laterally eroded into the bedrock. This more or less stable state ended with the abandonment of the prominent T1' terrace. During the second phase, the incision rate increased in both the foreland and the hinterland and has been dominated by down-cutting instead of lateral erosion. Due to this change in incision rate, only local inset terraces were formed during this phase. It is also during this phase that tributary knickzones started to form in response to the increasing incision rate of the main stem. We also suggest that channel incision into bedrock began during this second phase, based on the following evidence. First, bedrock outcrops occur as high as 10 m below the mapped remnants of the 9.5 kyr T1' tread. Second, mapping of the T1 terrace fill shows that prior to formation of T1', the Beida River had cut laterally into bedrock along the western side of its canyon over the 3.6 km

reach immediately upstream of the mountain front (Fig. 5). Post-T1' incision occurred in this area, preserving the T1 paleochannel axis and much of its buried canyon wall below the T1 and T1' terraces. The post-9.5 kyr BP increase in incision rate thus led to isolation of the river course within the bedrock below T1'.

Based on the slope patch theory for bedrock incision, we associate the three slope patches along the bedrock channel of the Beida River as formed during three incision stages over the second phase, since 9.5 kyr BP. In our model, each patch is projected to the mountain front outlet where the bedrock channel transitions to an alluvial channel. During the first stage, a relatively slow incision rate in the foreland formed the gentle slope and wide channel of patch 1. During the second stage, incision rate increased drastically in the foreland, which led to the formation of a steeper, narrower patch 2. During the third stage, incision rate in the foreland decreased, forming the youngest patch 3 with a gentle slope and wider channel, while the steeper patch 2 retreated upstream, replacing patch 1 (Fig. 7). Combined with the terrace records, we therefore define the first incision stage to occur from 9.5 kyr to sometime around 4.7 kyr BP, because the incision rates from 9.5 to 6.9 kyr BP and 6.9 to 4.7 kyr BP are identical within error, between $\sim$ 5–6 m kyr^{-1} (Fig. 6). This is followed by the second stage, with an incision rate of at least $\sim$ 25 m kyr. The third, present stage, started at or before 3.2 kyr BP with an incision rate of $\sim$ 12 m kyr^{-1}. Because the starting time and the duration of stage 2 is not well constrained due to the sparse terrace record, it is possible that stage 2 has a shorter duration than 1.5 kyr and its $\sim$ 25 m kyr^{-1} incision rate should be considered a minimum.

In addition to our terrace chronology, a three-stage incision history is also supported by the relative preservation of terraces along the Beida River, with a notable absence of terraces preserved between 40 and 80 m above river level (75 and 30 m below T1, Fig. 3b) within the foreland, during the period of most rapid incision inferred from the bracketing terrace record. These three incision stages have also left their imprints in the tributary knickzones (Fig. 4). Steep knickzones, often ending at waterfalls, occur on tributaries below the main-stem knickzone, suggesting that when these tributary knickzones formed the main stem was incising very fast so that the incision rate of the tributaries could not keep pace. Gentler knickzones formed on tributaries that join upstream of the main-stem knickzone suggest a slower incision rate of the main stem here, as the main-stem knickzone has not yet retreated through this area. These tributary knickzones continue to grow in height and upstream extent, as the incision rate in the main stem is still fast at present.

5.3 Coupled incision model for knickzone formation

Geometric and timing relations for patches 1, 2, and 3 may be coupled to further constrain the duration and incision rate of the knickzone formation stage (stage 2). Here we formulate these relationships into two sets of constraints. Constraint 1 comes from the knickzone retreat process and the geometric relationship between patch 2 and 3. The effective base level of patch 2 (z_{b2}, Fig. 3c) is determined by the relative incision rate between patch 2 and patch 3, and the duration of the third stage. Based on Eq. (4), we have

$$z_{b2} = \left(I_3 - I_{2,3}\right) \times t_3. \tag{6a}$$

Because we may estimate I_3 and t_3 from the position of the youngest, 3.2 kyr BP terrace, and z_{b2} from projection of the patch 2 river profile to the mountain front, we may calculate the incision rate along patch 2 during stage 3, $I_{2,3}$ as

$$I_{2,3} = I_3 - z_{b2}/t_3. \tag{6b}$$

It is reasonable to assume that during the knickzone formation, the incision rate along patch 2 should be greater than the present incision rate, $I_2 > I_{2,3}$. With known I_3, t_3, and z_{b2} (see Table S4 for details), the minimum rate of incision during knickpoint formation, I_2, is 50 ± 17 m kyr-1 (2σ confidence).

To find the maximum duration for the time of knickpoint formation, t_2, we introduce a second set of constraints, derived from the total incision at the mountain front since 9.5 kyr BP and the total incision along patch 1 since 6.9 kyr should both match the observed terrace record:

$$\begin{aligned} H_{9.5\,\mathrm{kyr}} &= t_1 \times I_1 + t_2 \times I_2 + t_3 \times I_3 \\ &= I_1\,(9.5\,\mathrm{kyr} - t_2 - t_3) + I_2 t_2 + I_3 t_3 \end{aligned} \tag{7}$$

and

$$H_{6.9\,\mathrm{kyr}} = I_1\,(6.9\,\mathrm{kyr} - t_2 - t_3) + I_{1,2} t_2 + I_{1,3} t_3. \tag{8}$$

In addition, the geometric relationship between patch 1 and 2 should also be satisfied. The effective base level of patch 1 (z_{b1}) is determined by the relative incision rate between patch 1 and patch 2, and patch 1 and patch 3, and the durations of the second and third stage. Based on Eq. (5), we have

$$z_{b1} = \left(I_2 - I_{1,2}\right) t_2 + \left(I_3 - I_{1,3}\right) t_3. \tag{9}$$

Based on constraint 2 and $I_{2\min} = 50 \pm 17$ m kyr^{-1}, we calculate the maximum duration of the second stage as 680 ± 460 yr (2σ confidence), which is approximately half of the duration suggested by the terrace record alone. It is worth noting that because the t_3 we used in the calculation is based on a minimum age for the lowest terrace, the maximum duration of stage 2 may be even shorter and the minimum stage 2 incision rate at mountain front may be even faster than calculated here. In addition, though we are able to constrain the maximum duration of the second stage to $\sim$ 700 years, which suggests this $<$ 700 year event happened sometime between 4.7 and 3.2 kyr BP, we do not have enough data to pinpoint when this event occurred within this 1500-year time span.

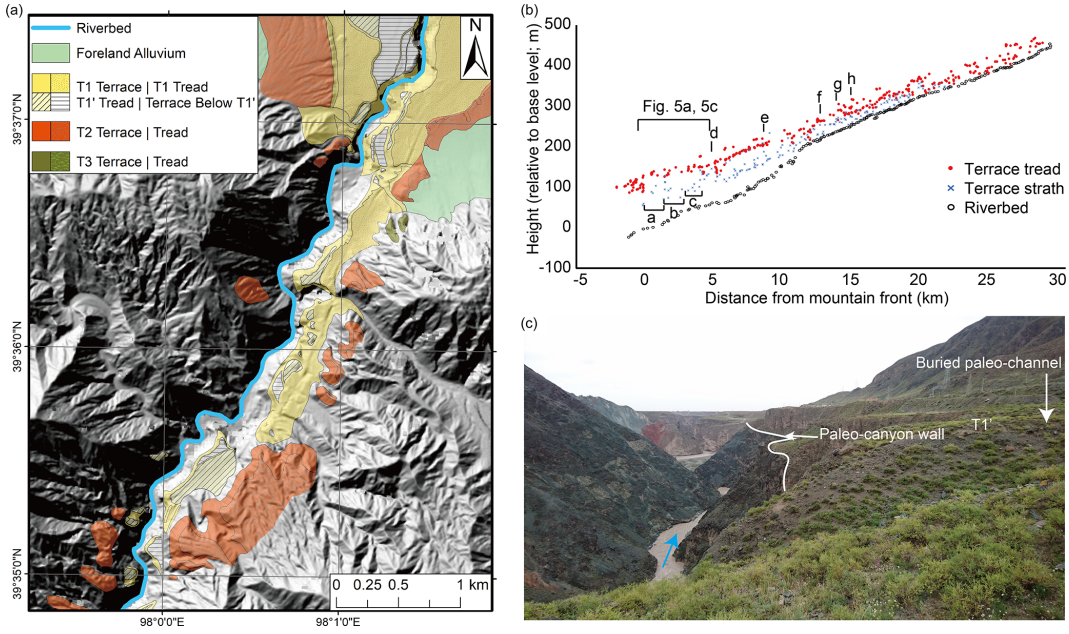

Figure 5. Bedrock incision and terrace preservation along the Beida River. **(a)** Terrace map of the lower reach of Beida River. T1 terraces are all preserved on the east side of the canyon. **(b)** Terrace profiles of Beida River. Letters correspond to reaches where terrace mapping indicates that the original paleocanyon is preserved and the river incised into the adjacent bedrock soon after the abandonment of T1' (see Fig. S5). **(c)** Photo of the lower reach of Beida River, looking downstream, with paleochannel axis and paleocanyon wall annotated. Here the river incised mostly into bedrock along the west edge of the T1 terrace fill deposit.

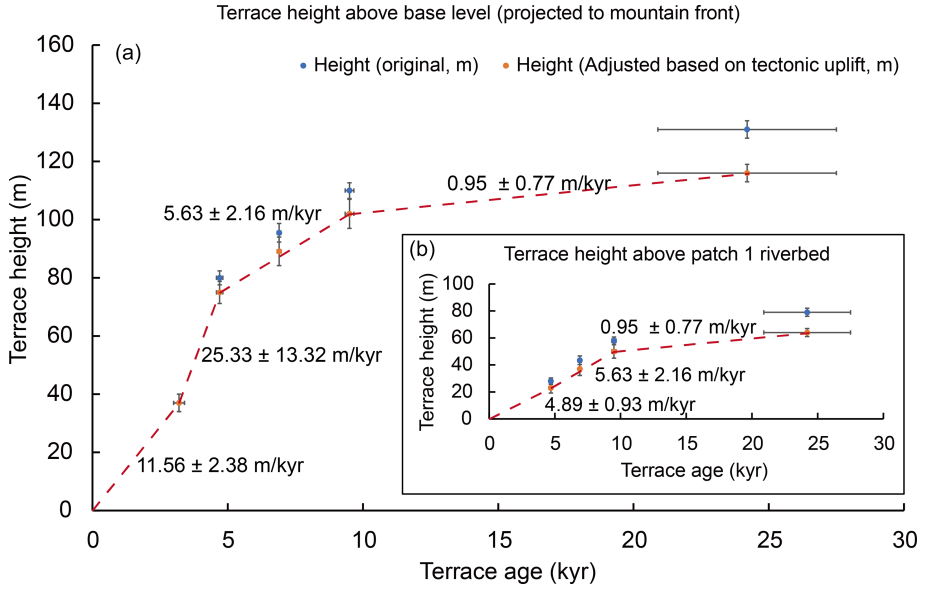

Figure 6. **(a)** Terrace height above base level and the incision rate of each stage at the mountain front. **(b)** Terrace height and incision rate of each stage above patch 1, upstream of the knickpoint. Details of elevations with correction for tectonic uplift are in Table 4.

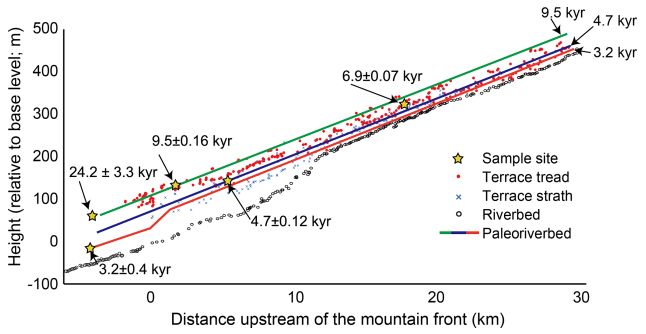

Figure 7. Simplified model for Beida River incision since 9.5 kyr. The surveyed terrace treads and the paleoriverbeds we projected are corrected for tectonic uplift and therefore slightly deviated from the sample locations. The time period between 24.2 and 9.5 kyr BP is not included in this model because the river was mostly incising into the T1 terrace fill, and therefore the incision of the foreland and hinterland should be synchronous.

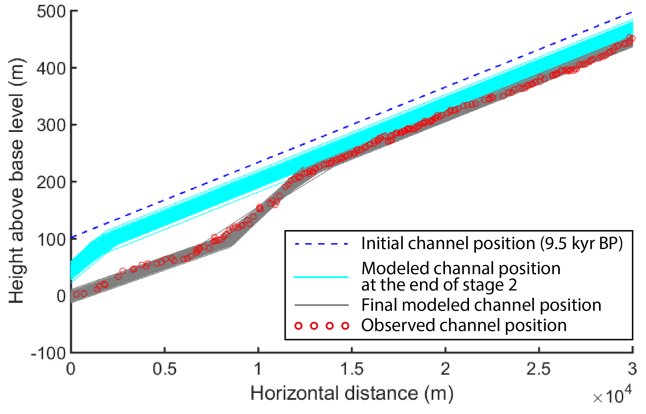

Figure 8. Monte Carlo simulation of channel position at the end of stage 2 and at present, end of stage 3, compared to the observed river profile. Results of 500 simulations are shown. Parameters for simulations were selected from valid model results for the timing, duration, and incision rate stages 2 and 3.

To verify these model results, we ran simulations of the channel evolution using our parameter estimations and compare this with our surveyed channel profile (Fig. 8). The simulation results fit well with the observed channel profile, while the modeled channel positions at the end of stage 2 have a relatively wide range of possible geometries because we have less control on the starting and ending time of stage 2. The simulation results therefore verify that the 680-year maximum duration and 50 m kyr^{-1} minimum second stage incision rate are good constraints for the Beida River incision history.

5.4 Climate implications of the Beida River incision history

Based on our prior study (Wang et al., 2020), the major T1 and T2 fill terraces of the Beida River correspond to the last glacial and penultimate glacial periods, respectively. A similar pattern occurs along the Hongshuiba River, the next major river to the east of the Beida River. The T1 terrace here is similar in age to T1 at the Beida River (26.5 ± 5.0 kyr in Yang et al., 2020; 22.5 ± 2.2 kyr in Hetzel et al., 2019), and the T4 terrace here has a similar age to the T2 terrace at the Beida River (153 ± 12 kyr in Hetzel et al., 2019). In the eastern North Qilian Shan, terrace records of the Shagou River also show a fill–cut pattern synchronized to glacial–interglacial cycles (Pan et al., 2003). Therefore, we suggest the formation of fill terraces along the major rivers draining the North Qilian Shan is controlled by the same mechanisms, linked to glacial–interglacial cycles. A full fill–cut cycle begins with the river backfilling its canyon with sediment during the glacial period. This is a period with elevated, glacially derived sediment flux, and perhaps a drier climate and lower discharge than at present. At the glacial–interglacial transition, the river transitions from deposition to erosion as sediment supply gradually declines. This corresponds to the first incision phase of the Beida River (24–9.5 kyr BP). The fast, second incision phase of the Bieda River starting after 9.5 kyr BP corresponds in time with highstands of several endorheic lakes located in northwestern China including the Juyanze paleolake, which have been interpreted as a signal of intensification of monsoon influence (i.e., Herzschuh et al., 2006; Hartmann and Wünnemann, 2009; Jiang et al, 2008; Li et al, 2009; Rhodes et al, 1996; Wang et al, 2013). Therefore, the post-9.5 ka fast incision phase may relate to a regional increase in discharge, beginning near the end of the last glacial termination, as a result of the introduction of monsoon-derived summer moisture.

The mid-Holocene $< 680 \pm 460$-year event which punctuated the moderately fast incision of the Beida River since 9.5 kyr BP seems to be a result of an unusual short-term hydrologic perturbation. Similar knickzones found in other western North Qilian rivers, i.e., Hongshuiba River and Maying River (Fig. 1), suggest that this was a regional event that affected the entire western North Qilian Shan. We suggest this short-term hydrologic anomaly was driven by an increase in precipitation as a result of increased monsoon influence, and possibly enhanced by glacial melt due to warmer temperatures. Records of the terminal Juyanze paleolake suggest the highest mid-Holocene lake level occurred at 4.2 kyr BP (Hartmann and Wünnemann, 2009), and pollen records of the same area suggest a wet or pluvial period between 5.4 and 3.9 kyr BP (Herzschuh et al., 2004). Regionally, evidence for similar humid periods can also be found from Zhuyeze, a lake fed by Shiyang River of the eastern North Qilian Shan (Chen et al., 2006), Qinghai Lake (Chen et al., 2016) located within the southeast Qilian Shan, Tianchi Lake of Li-

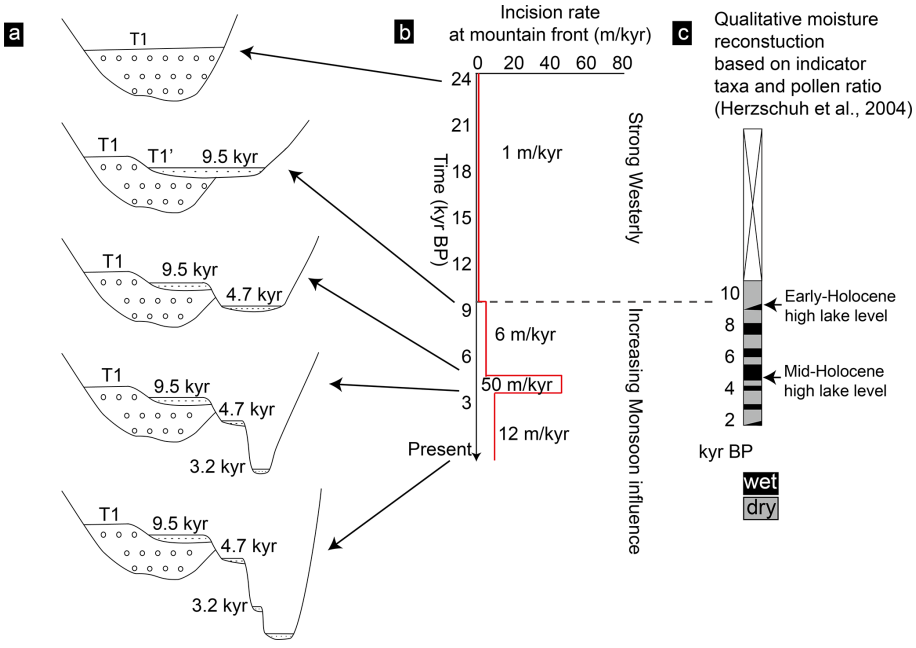

Figure 9. **(a)** Schematic cross sections of Beida River channel evolution at the mountain front. **(b)** Diagram of incision rate vs. time since 24 kyr BP. **(c)** Climate reconstruction based on the Eastern Juyanze paleolake record (Herzschuh et al., 2004).

upan Shan (Zhou et al., 2010), and Yanhaizi Lake of Inner Mongolia (Chen et al., 2003). Cave records from the upper Hanjiang region and Qinling Mountains (Tan et al., 2018) and stratigraphic sections from the Loess Plateau also support the existence of a mid-Holocene humid period (Fang et al., 1999, 2003; Chen et al., 1997; Xiao et al., 2002). All of this evidence suggests there was a humid period during the mid-Holocene that correlates well with our stage 2 rapid incision period. Considering the western North Qilian Shan is located at the transition zone between the Southeast Asian Monsoon and mid-latitude westerlies, and that wet periods regionally correspond to increased monsoon influence (Chen et al., 2018; Tan et al., 2018), we hypothesize that the < 700-year incision event on the Beida River occurred at the peak of monsoon influence within the region.

In summary, combining all the circumstantial evidence documented here, we suggest the Beida River experienced the following incision and climate history since 24 kyr BP. After 24 kyr, the river started to incise as it gradually depleted its sediment supply during the deglaciation and early interglacial period. Its incision rate (corrected for uplift) of $1.0 \pm 0.8\,\mathrm{m\,kyr^{-1}}$ was more or less in balance with the rock uplift rate during this time. During the Early Holocene, the humid Southeast Asian Monsoon expanded to the central North Qilian Shan, where it affected the Hei He drainage and filled Juyanze lake to a high lake level. The expanded monsoon correlates to the first incision stage of the Beida River when the canyon incised at a rate of $5.6 \pm 2.2\,\mathrm{m\,kyr^{-1}}$. During the mid-Holocene, the monsoon influence grew stronger, leading to a regional pluvial period. This peak of monsoon influence lasted less than 680 ± 460 years in the Beida River drainage, which led to an increase in precipitation, and therefore an increase in water discharge and incision rate. This climate event led to deepening of canyons into the foreland basin and prompted the formation of bedrock knickzones in the Maying, Hongshuiba, and Beida River sub-basins of the Hei He. During this pluvial period, the incision rate of the Bieda River increased to at least $50 \pm 17\,\mathrm{m\,kyr^{-1}}$. Afterward, the discharge decreased to its present condition and river incision slowed to $11.6 \pm 1.4\,\mathrm{m\,kyr^{-1}}$ (Fig. 9).

Though we hypothesize that knickzones present on the Hongshuiba River and Maying River also formed at the mountain front during a mid-Holocene pluvial period, the consistent locations of these knickzones 7–13 km upstream of the mountain front (Fig. S7a(1)–c(1)) is somewhat surprising, considering the dissimilar sizes of these drainage basins (Table 1). One might expect that the knickzones on the Hongshuiba River and Maying River would have retreated less, as these drainage basins are smaller than that of the Beida River (Table 1). Normalizing by upstream drainage area to produce a χ plot (Perron and Royden, 2013) of these rivers (Fig. S7a(2)–c(2)) confirms that the knickzone location on the Maying River has retreated about twice this normalized distance upstream relative to the Hongshuiba River. Likewise, the knickzone on the Hongshuiba River is about 1.5 times this normalized distance upstream relative to the Beida River. We suggest this pattern of greater knickzone retreat from west to east is partially the result of the strong west-to-east precipitation gradient present within the western North Qilian Shan. Normalizing by the ratio of discharge per unit

drainage area at the mountain front (Table 1), relative to the Beida River, partially accounts for the difference in knickzone positions on the Hongshuiba River and Maying River (Fig. S7a(3)–c(3)). It is worth noting that, though precipitation gradient related to elevation has the potential of further reducing the normalized knickzone retreating distance of the Hongshuiba and Maying rivers, we are unable to incorporate this effect into the adjusted χ plots due to a lack of detailed precipitation data. Both the timing and amount of precipitation during the mid-Holocene pluvial period could account for the remaining difference. The mid-Holocene highstand of the terminal Juyanze paleolake precedes the very rapid incision of the Beida River by a few hundred years (Fig. 9, Herzschuh et al., 2004), which suggests that the pluvial period may have begun earlier in the eastern part of the Hei He drainage basin. This is consistent with the observation that both the Hongshuiba and Maying rivers canyons are incised deeper into the foreland basin than the Beida River, indicating an even faster integrated rate of Holocene incision. It is also possible that the west-to-east precipitation gradient was stronger during the early and mid-Holocene than at present. Because knickzone retreat rate will be faster for steeper, narrower channels (Finnegan et al., 2005), the rate of abrupt base level drop should affect the rate of retreat of these knickzones. Contrary to the large rivers, lesser streams draining across the mountain front and the Beida River tributaries do not exhibit evidence for deep, rapid incision. We attribute this difference to the aridity at lower elevation and the fact that only those drainages that tap high elevations (over 4000 m) are supplied continuously during the summer by glacier melt. In summary, variations in discharge, due both to monsoon influence and orographic effects, strongly impacts the Holocene incision rate and evolutionary pattern of both major and small rivers draining the western North Qilian Shan.

6 Conclusions

The Beida River in the North Qilian Shan has incised deeply into both the bedrock and the adjacent foreland basin sediments. The incision rates indicated from terrace records and our models greatly exceed rates of tectonic uplift here. Our work demonstrates the capability of bedrock rivers in arid regions to incise deep channels and form fast retreating knickpoints within a short period. Field investigation and geomorphic mapping identify a 24 kyr fill terrace, T1, and several sets of inset terraces below. The longitudinal profile of the present river channel preserves a steep knickzone, located 10 to 12 km upstream of the mountain front. Terrace ages, and relationships between terrace treads and the riverbed, indicate that the knickzone was formed quickly after 4.7 kyr BP, likely driven by an increase in river discharge. By applying the concept of slope patches along with channel geometry and terrace records, we constrain that during the knickzone formation, the incision rate was at least $50 \pm 17\,\mathrm{m\,kyr^{-1}}$ and the duration of this period of increased discharge was less than 680 ± 460 year, which is about half of that estimated from the sparse terrace age record alone. The period of increased incision rate identified from the Beida River correlates to a pluvial period recorded at the terminal Juyanze lake. The likely cause of rapid incision of the Beida River, and adjacent rivers with similar deeply incised canyons, is the increased influence of the Southeast Asian Monsoon over the Holocene, with the most rapid incision period corresponding to a peak of monsoon influence ca. 4 to 5 kyr BP.

Data availability. We placed the supplement materials and data in a permanent repository at Open Science Framework (https://osf.io/bpvw9/) (Wang, 2020).

Supplement. The supplement related to this article is available online at: https://doi.org/10.5194/esurf-10-191-2022-supplement.

Author contributions. The fieldwork was conducted with contributions from all four authors. HZ contribute to OSL sampling and dating. YW, MEO, and YL contribute to carbon sample collection and dating. YW developed the incision model and conducted the simulation with advice from MEO. YW prepared the paper along with MEO. YL and HZ have also contributed to the completion of the paper.

Competing interests. The contact author has declared that neither they nor their co-authors have any competing interests.

Disclaimer. Publisher's note: Copernicus Publications remains neutral with regard to jurisdictional claims in published maps and institutional affiliations.

Acknowledgements. This work was supported by the US National Science Foundation (grant number EAR-1524734) to Michael Oskin, the National Natural Science Foundation of China (grant number 41571001) to Youli Li, the Second Tibetan Plateau Scientific Expedition and Research (STEP) (grant number 2019QZKK0704) and the National Natural Science Foundation of China (grant number 41622204; 41761144071) to Huiping Zhang, and through the Cordell Durrell Geology Field Fund to Yiran Wang. We thank the associate editor, Richard Gloaguen, and the referees, Wolfgang Schwanghart, Richard Ott, Sean Gallen, and Christopher Sheehan, for their valuable comments that helped us greatly improve the quality of our paper.

Financial support. This research has been supported by the National Science Foundation (grant no. EAR-1524734), the National Natural Science Foundation of China (grant nos.

41571001, 41622204, and 41761144071), and the Second Tibetan Plateau Scientific Expedition and Research (STEP) (grant no. 2019QZKK0704).

Review statement. This paper was edited by Richard Gloaguen and reviewed by Wolfgang Schwanghart, Christopher Sheehan, Sean Gallen, and Richard Ott.

References

An, Z., Kutzbach, J. E., Prell, W. L., and Porter, S. C.: Evolution of Asian monsoons and phased uplift of the Himalaya – Tibetan plateau since Late Miocene times, Nature, 411, 62–66, https://doi.org/10.1038/35075035, 2001.

Attal, M., Cowie, P. A., Whittaker, A. C., Hobley, D., Tucker, G. E., and Roberts, G. P.: Testing fluvial erosion models using the transient response of bedrock rivers to tectonic forcing in the Apennines, Italy, J. Geophys. Res.-Earth, 116, 1–17, https://doi.org/10.1029/2010JF001875, 2011.

Berlin, M. M. and Anderson, R. S.: Modeling of knickpoint retreat on the Roan Plateau, western Colorado, J. Geophys. Res.-Earth, 112, 1–16, https://doi.org/10.1029/2006JF000553, 2007.

Bishop, P., Hoey, T. B., Jansen, J. D., and Lexartza Artza, I.: Knickpoint recession rate and catchment area: The case of uplifted rivers in Eastern Scotland, Earth Surf. Proc. Land., 30, 767–778, https://doi.org/10.1002/esp.1191, 2005.

Chen, C. T. A., Lan, H. C., Lou, J. Y., and Chen, Y. C.: The dry Holocene Megathermal in Inner Mongolia, Palaeogeogr. Palaeocl., 193, 181–200, https://doi.org/10.1016/S0031-0182(03)00225-6, 2003.

Chen, F., Bloemendal, J., Wang, J. M., Li, J. J., and Oldfield, F.: High-resolution multi-proxy climate records from Chinese Loess: Evidence for rapid climatic changes over the last 75 kyr, Palaeogeogr. Palaeocl., 130, 323–335, https://doi.org/10.1016/S0031-0182(96)00149-6, 1997.

Chen, F., Cheng, B., Zhao, Y., Zhu, Y., and Madsen, D. B.: Holocene environmental change inferred from a high-resolution pollen record, Lake Zhuyeze, arid China, Holocene, 16, 675–684, https://doi.org/10.1191/0959683606hl951rp, 2006.

Chen, F., Wu, D., Chen, J., Zhou, A., Yu, J., Shen, J., Wang, S., and Huang, X.: Holocene moisture and East Asian summer monsoon evolution in the northeastern Tibetan Plateau recorded by Lake Qinghai and its environs: A review of conflicting proxies, Quaternary Sci. Rev., 154, 111–129, https://doi.org/10.1016/j.quascirev.2016.10.021, 2016.

Chen, R., Han, C., Liu, J., Yang, Y., Liu, Z., Wang, L., and Kang, E.: Maximum precipitation altitude on the northern flank of the Qilian Mountains, northwest China, Hydrol. Res., 49, 1696–1710, https://doi.org/10.2166/nh.2018.121, 2018.

Crosby, B. T. and Whipple, K. X.: Knickpoint initiation and distribution within fluvial networks: 236 waterfalls in the Waipaoa River, North Island, New Zealand, Geomorphology, 82, 16–38, https://doi.org/10.1016/j.geomorph.2005.08.023, 2006.

Fang, X., Lü, L., Mason, J. A., Yang, S., An, Z., Li, J., and Zhilong, G.: Pedogenic response to millennial summer monsoon enhancements on the Tibetan Plateau, Quatern. Int., 106–107, 79–88, https://doi.org/10.1016/S1040-6182(02)00163-5, 2003.

Fang, X. M., Ono, Y., Fukusawa, H., Bao-Tian, P., Li, J. J., Dong-Hong, G., Oi, K., Tsukamoto, S., Torii, M., and Mishima, T.: Asian summer monsoon instability during the past 60,000 years: Magnetic susceptibility and pedogenic evidence from the western Chinese Loess Plateau, Earth Planet. Sc. Lett., 168, 219–232, https://doi.org/10.1016/S0012-821X(99)00053-9, 1999.

Finnegan, N. J., Roe, G., Montgomery, D. R., and Hallet, B.: Controls on the channel width of rivers: Implications for modeling fluvial incision of bedrock, Geology, 33, 229–232, https://doi.org/10.1130/G21171.1, 2005.

Finnegan, N. J., Sklar, L. S., and Fuller, T. K.: Interplay of sediment supply, river incision, and channel morphology revealed by the transient evolution of an experimental bedrock channel, J. Geophys. Res.-Earth, 112, F03S11, https://doi.org/10.1029/2006JF000569, 2007.

Gansu Province Local Chronicles Compilation Committee: Gansu Provincial Chronicle: Water Resources, Gansu Cultural Publishing House, Lanzhou, China, 57, 31–33, 1998 (In Chinese).

Geng, H., Pan, B., Huang, B., Cao, B., and Gao, H.: The spatial distribution of precipitation and topography in the Qilian Shan Mountains, northeastern Tibetan Plateau, Geomorphology, 297, 43–54, https://doi.org/10.1016/j.geomorph.2017.08.050, 2017.

Guo, W., Xu, J., Liu, S., Shangguan, D., Wu, L., Yao, X., Zhao, J., Liu, Q., Jiang, Z., Li, P., Wei, J., Bao, W., Yu, P., Ding, L., Li, G., Ge, C., and Wang, Y.: The Second Glacier Inventory Dataset of China (Version 1.0), National Tibetan Plateau Data Center [data set], https://doi.org/10.3972/glacier.001.2013.db, 2014.

Hartmann, K. and Wünnemann, B.: Hydrological changes and Holocene climate variations in NW China, inferred from lake sediments of Juyanze palaeolake by factor analyses, Quatern. Int., 194, 28–44, https://doi.org/10.1016/j.quaint.2007.06.037, 2009.

Haviv, I., Enzel, Y., Whipple, K. X., Zilberman, E., Stone, J., Matmon, A., and Fifield, L. K.: Amplified erosion above waterfalls and oversteepened bedrock reaches, J. Geophys. Res.-Earth, 111, 1–11, https://doi.org/10.1029/2006JF000461, 2006.

He, P., Song, C., Wang, Y., Chen, L., Chang, P., Wang, Q., and Ren, B.: Cenozoic exhumation in the Qilian Shan, northeastern Tibetan Plateau: Evidence from detrital fission track thermochronology in the Jiuquan Basin, J. Geophys. Res.-Sol. Ea., 122, 6910–6927, https://doi.org/10.1002/2017JB014216, 2017.

He, P., Song, C., Wang, Y., Wang, D., Chen, L., Meng, Q., and Fang, X.: Early Cenozoic activated deformation in the Qilian Shan, northeastern Tibetan Plateau: Insights from detrital apatite fission-track analysis, Basin Res., 33, 1731–1748, https://doi.org/10.1111/bre.12533, 2021.

Herzschuh, U., Tarasov, P., Wünnemann, B., and Hartmann, K.: Holocene vegetation and climate of the Alashan Plateau, NW China, reconstructed from pollen data, Palaeogeogr. Palaeocl., 211, 1–17, https://doi.org/10.1016/j.palaeo.2004.04.001, 2004.

Herzschuh, U., Kürschner, H., and Mischke, S.: Temperature variability and vertical vegetation belt shifts during the last $\sim 50,000$ yr in the Qilian Mountains (NE margin of the Tibetan Plateau, China), Quaternary Res., 66, 133–146, https://doi.org/10.1016/j.yqres.2006.03.001, 2006.

Hetzel, R., Hampel, A., Gebbeken, P., Xu, Q., and Gold, R. D.: A constant slip rate for the western Qilian Shan frontal thrust during the last 200 ka consistent with GPS-derived and geo-

logical shortening rates, Earth Planet. Sc. Lett., 509, 100–113, https://doi.org/10.1016/j.epsl.2018.12.032, 2019.

Hu, G., Yi, C., Zhang, J., Liu, J., Jiang, T., and Qin, X.: Optically stimulated luminescence dating of a moraine and a terrace in Laohugou valley, western Qilian Shan, northeastern Tibet, Quatern. Int., 321, 37–49, https://doi.org/10.1016/j.quaint.2013.12.019, 2014.

Jiang, Q., Shen, J., Liu, X., and Zhang, E.: Holocene climate reconstructions of Ulungur Lake (Xinjiang, China) inferred from ostracod species assemblages and stable isotopes, Frontiers of Earth Science in China, 2, 31–40, https://doi.org/10.1007/s11707-008-0007-z, 2008.

Jolivet, M., Brunel, M., Seward, D., Xu, Z., Yang, J., Roger, F., Tapponnier, P., Malavieille, J., Arnaud, N., and Wu, C.: Mesozoic and Cenozoic tectonics of the northern edge of the Tibetan plateau: Fission-track constraints, Tectonophysics, 343, 111–134, https://doi.org/10.1016/S0040-1951(01)00196-2, 2001.

Küster, Y., Hetzel, R., Krbetschek, M., and Tao, M.: Holocene loess sedimentation along the Qilian Shan (China): Significance for understanding the processes and timing of loess deposition, Quaternary Sci. Rev., 25, 114–125, https://doi.org/10.1016/j.quascirev.2005.03.003, 2006.

Lamb, M. P., Finnegan, N. J., Scheingross, J. S., and Sklar, L. S.: New insights into the mechanics of fluvial bedrock erosion through flume experiments and theory, Geomorphology, 244, 33–55, https://doi.org/10.1016/j.geomorph.2015.03.003, 2015.

Lavé, J. and Avouac, J. P.: Active folding of fluvial terraces across the Siwaliks Hills, Himalayas of central Nepal, J. Geophys. Res., 105, 5735–5770, https://doi.org/10.1029/1999JB900292, 2000.

Li, Y., Wang, N., Cheng, H., Long, H., and Zhao, Q.: Holocene environmental change in the marginal area of the Asian monsoon: A record from Zhuye Lake, NW China, Boreas, 38, 349–361, https://doi.org/10.1111/j.1502-3885.2008.00063.x, 2009.

Meng, X., Zhang, S., and Zhang, Y.: The Temporal and Spatial Change of Temperature and Precipitation in Hexi Corridor in Recent 57 Years, Acta Geol. Sin.-Engl., 67, 1482–1492, 2012.

Merritts, D. J., Vincent, K. R., and Wohl, E. E.: Long river profiles, tectonism, and eustasy: a guide to interpreting fluvial terraces, J. Geophys. Res., 99, 14031–14050, https://doi.org/10.1029/94jb00857, 1994.

Mischke, S., Fuchs, D., Riedel, F., and Schudack, M. E.: Mid to Late Holocene palaeoenvironment of Lake Eastern Juyanze (northwestern China) based on ostracods and stable isotopes, Geobios, 35, 99–110, 2002.

Mischke, S., Demske, D., Wünnemann, B., and Schudack, M. E.: Groundwater discharge to a Gobi desert lake during Mid and Late Holocene dry periods, Palaeogeogr. Palaeocl., 225, 157–172, https://doi.org/10.1016/j.palaeo.2004.10.022, 2005.

Owen, L. A., Spencer, J. Q., Haizhou, M., Barnard, P. L., Derbyshire, E., Finkel, R. C., Caffee, M. W., and Nian, Z. Y.: Timing of Late Quaternary glaciation along the southwestern slopes of the Qilian Shan, Tibet, Boreas, 32, 281–291, https://doi.org/10.1111/j.1502-3885.2003.tb01083.x, 2003.

Pan, B., Burbank, D. W., Wang, Y., Wu, G., Li, J., and Guan, Q.: A 900 k.y. record of strath terrace formation during glacial-interglacial transitions in northwest China, Geology, 31, 957–960, https://doi.org/10.1130/G19685.1, 2003.

Perron, J. T. and Royden, L.: An integral approach to bedrock river profile analysis, Earth Surf. Proc. Land., 38, 570–576, https://doi.org/10.1002/esp.3302, 2013.

Qiang, F., Zhang, M., Wang, S., Liu, Y., Ren, Z., and Zhu, X.: Estimation of areal precipitation in the Qilian Mountains based on a gridded dataset since 1961, J. Geogr. Sci., 26, 59–69, https://doi.org/10.1007/s11442-016-1254-7, 2016.

Raup, B., Racoviteanu, A., Khalsa, S. J. S., Helm, C., Armstrong, R., and Arnaud, Y.: The GLIMS geospatial glacier database: A new tool for studying glacier change, Global. Planet. Change, 56, 101–110, https://doi.org/10.1016/j.gloplacha.2006.07.018, 2007.

Reimer, P., Bard, E., Bayliss, A., Beck, J., Blackwell, P., Ramsey, C. B., Grootes, P., Guilderson, T., Haflidason, H., Hajdas, I., Hatté, C., Heaton, T., Hoffmann, D., Hogg, A., Hughen, K., Kaiser, K., Kromer, B., Manning, S., Niu, M., Reimer, R., Richards, D., Scott, E., Southon, J., Staff, R., Turney, C., and van der Plicht, J.: IntCal13 and Marine13 Radiocarbon Age Calibration Curves 0–50,000 Years cal BP, Radiocarbon, 55, 1869–1887, 2013.

Rhodes, T. E., Gasse, F., Lin, R., Fontes, J. C., Wei, K., Bertrand, P., Gibert, E., Mélières, F., Piotr, T., Wang, Z., and Cheng, Z. Y.: A Late Pleistocene-Holocene lacustrine record from Lake Manas, Zunggar (northern Xinjiang, western China), Palaeogeogr. Palaeocl., 120, 105–121, https://doi.org/10.1016/0031-0182(95)00037-2, 1996.

Royden, L. and Perron, J. T.: Solutions of the stream power equation and application to the evolution of river longitudinal profiles, J. Geophys. Res.-Earth, 118, 497–518, https://doi.org/10.1002/jgrf.20031, 2013.

Shean, D.: High Mountain Asia 8-meter DEM Mosaics Derived from Optical Imagery, Version 1, tile-224, tile-257, Boulder, Colorado USA, NASA National Snow and Ice Data Center Distributed Active Archive Center [data set], https://doi.org/10.5067/KXOVQ9L172S2, 2017.

Shi, Y.: New Understanding of Quaternary Glaciations in China, Shanghai Popular Science Press, Shanghai, China, 2011 (in Chinese).

Shi, Y., Cui, Z., and Su, Z.: The Quaternary Glaciations and Environmental Variations in China, Hebei Science and Technology Press, Shijiazhuang, China, 2006 (in Chinese).

Sun, M., Liu, S., Yao, X., Guo, W., and Xu, J.: Glacier changes in the Qilian Mountains in the past half century: Based on the revised First and Second Chinese Glacier Inventory, Acta Geographica Sinica, 70, 1402–1414, https://doi.org/10.11821/dlxb201509004, 2015 (in Chinese with English Abstract).

Tan, L., Cai, Y., Cheng, H., Edwards, L. R., Gao, Y., Xu, H., Zhang, H., and An, Z.: Centennial- to decadal-scale monsoon precipitation variations in the upper Hanjiang River region, China over the past 6650 years, Earth Planet. Sc. Lett., 482, 580–590, https://doi.org/10.1016/j.epsl.2017.11.044, 2018.

Tapponnier, P., Xu, Z., Roger, F., Meyer, B., Arnaud, N., Wittlinger, G., and Yang, J.: Oblique stepwise rise and growth of the tibet plateau, Science, 294, 1671–1677, https://doi.org/10.1126/science.105978, 2001.

Tucker, G. E. and Whipple, K. X.: Topographic outcomes predicted by stream erosion models: Sensitivity analysis and intermodel comparison, J. Geophys. Res.-Sol. Ea., 107, ETG 1-1–ETG 1-16, https://doi.org/10.1029/2001JB000162, 2002.

Turowski, J. M., Lague, D., and Hovius, N.: Cover effect in bedrock abrasion: A new derivation and its implications for the modeling of bedrock channel morphology, J. Geophys. Res.-Earth, 112, F04006, https://doi.org/10.1029/2006JF000697, 2007.

Wang, W., Feng, Z., Ran, M., and Zhang, C.: Holocene climate and vegetation changes inferred from pollen records of Lake Aibi, northern Xinjiang, China: A potential contribution to understanding of Holocene climate pattern in East-central Asia, Quatern. Int., 311, 54–62, https://doi.org/10.1016/j.quaint.2013.07.034, 2013.

Wang, Y.: Rapid bedrock canyon incision during a mid-Holocene pluvial period, Qilian Shan, China, OSFHOME [data set], https://osf.io/bpvw9/, last access: 9 March 2020.

Wang, Y., Oskin, M. E., Zhang, H., Li, Y., Hu, X., and Lei, J.: Deducing crustal-scale reverse-fault geometry and slip distribution from folded river terraces, Qilian Shan, China, Tectonics, 39, 1–18, https://doi.org/10.1029/2019TC005901, 2020.

Wei, K. and Gasse, F.: Oxygen isotopes in lacustrine carbonates of West China revisited: Implications for post glacial changes in summer monsoon circulation, Quaternary Sci. Rev., 18, 1315–1334, https://doi.org/10.1016/S0277-3791(98)00115-2, 1999.

Whipple, K. X. and Tucker, G. E.: Dynamics of the stream-power river incision model: Implications for height limits of mountain ranges, landscape response timescales, and research needs, J. Geophys. Res.-Sol. Ea., 104, 17661–17674, https://doi.org/10.1029/1999JB900120, 1999.

Whittaker, A. C.: How do landscapes record tectonics and climate?, Lithosphere, 4, 160–164, https://doi.org/10.1130/RF.L003.1, 2012.

Wobus, C., Whipple, K. X., Kirby, E., Snyder, N., Johnson, J., Spyropolou, K., Crosby, B., and Sheehan, D.: Tectonics from topography: Procedures, promise, and pitfalls, Special Papers, Geol. S. Am. S., 2398, 55–74, https://doi.org/10.1130/2006.2398(04), 2006.

Wohl, E. and David, G. C. L.: Consistency of scaling relations among bedrock and alluvial channels, J. Geophys. Res.-Earth, 113, 1–16, https://doi.org/10.1029/2008JF000989, 2008.

Xiao, J., Nakamura, T., Lu, H., and Zhang, G.: Holocene climate changes over the desert/loess transition of north-central China, Earth Planet. Sc. Lett., 197, 11–18, https://doi.org/10.1016/S0012-821X(02)00463-6, 2002.

Yang, H., Yang, X., Huang, W., Li, A., Hu, Z., Huang, X., and Yang, H.: ^{10}Be and OSL dating of Pleistocene fluvial terraces along the Hongshuiba River: Constraints on tectonic and climatic drivers for fluvial downcutting across the NE Tibetan Plateau margin, China, Geomorphology, 348, 106884, https://doi.org/10.1016/j.geomorph.2019.106884, 2020.

Zhao, J. D., Zhou, S. Z., Cui, J. X., Pan, X. D., Xu, L. B., and Zhang, X. W.: ESR chronology of Bailanghe Valley and new understanding of Qilian Shan Mountain's Quaternary glaciation, J. Mt. Sci., 19, 481–488, 2001 (in Chinese).

Zheng, D., Clark, M. K., Zhang, P., Zheng, W., and Farley, K. A.: Erosion, fault initiation and topographic growth of the North Qilian Shan (northern Tibetan Plateau), Geosphere, 6, 937–941, https://doi.org/10.1130/GES00523.1, 2010.

Zhou, A., Sun, H., Chen, F., Zhao, Y., An, C., Dong, G., Wang, Z., and Chen, J.: High-resolution climate change in mid-late Holocene on Tianchi Lake, Liupan Mountain in the Loess Plateau in central China and its significance, Chinese Science Bulletin, 55, 2118–2121, https://doi.org/10.1007/s11434-010-3226-0, 2010.

Zhou, S., Li, J., and Zhang, S.: Quaternary glaciation of the Bailang River Valley, Qilian Shan, Quatern. Int., 97–98, 103–110, https://doi.org/10.1016/S1040-6182(02)00055-1, 2002.